

Structure and Magnetic Properties of Monodisperse Fe³⁺-doped CeO₂ Nanospheres

Sumalin Phokha¹, Supree Pinitsoontorn¹, Santi Maensiri^{2,*}

(Received 4 July 2013; accepted 18 September 2013; published online 15 October 2013)

Abstract: This work reports the study concerning the structure and magnetic properties of undoped CeO₂ and Fe-doped CeO₂ (Ce_{1-x}Fe_xO₂, 0.01 ≤ x ≤ 0.07) nanospheres with diameters of 100~200 nm prepared by hydrothermal method using polyvinylpyrrolidone (PVP) as surfactant. The prepared samples were studied by using X-ray diffraction (XRD), Raman spectroscopy, transmission electron microscopy (TEM), high-resolution transmission electron microscopy (HRTEM), X-ray absorption near-edge structure (XANES), and vibrating sample magnetometry (VSM). The XRD results showed that Fe-doped CeO₂ was single-phased with a cubic structure, and with Fe³⁺ successfully substituting in Ce⁴⁺ sites. Raman spectra showed a redshift of F_{2g} mode that caused by the Fe doping. The samples of both undoped CeO₂ and Fe-doped CeO₂ exhibited room temperature ferromagnetism, and the saturated magnetization (M_s) increased with increasing Fe content until x = 0.05, and then the samples displayed ferromagnetic loops as well as paramagnetic behavior. The roles of Ce³⁺ and Fe³⁺ spin electrons are discussed for the ferromagnetism in the Fe-doped CeO₂.

Keywords: Cerium oxide; Nanospheres; Dilute magnetic oxide; Ferromagnetism; Oxygen vacancies; XANES

Citation: Sumalin Phokha, Supree Pinitsoontorn and Santi Maensiri, "Structure and Magnetic Properties of Monodisperse Fe³⁺-doped CeO₂ Nanospheres", Nano-Micro Lett. 5(4), 223-233 (2013). <http://dx.doi.org/10.5101/nml.v5i4.p223-233>

Introduction

Oxide-dilute magnetic semiconductors (O-DMSs) are materials that exhibit ferromagnetic (FM) at room temperature (RT) with a Curie temperature above RT. These O-DMSs are also optically transparent and can be used for the development in spintronic devices [1,2]. Sine devices use both the spin and the charge of electrons can be controlled with an external magnetic field. Many studies report that these O-DMSs display RT-FM in transition metals (TMs) doping when grown as thin films [3] or in powder form [4]. The carrier-induced FM mechanism is used to explain the FM in semiconducting oxides. In some systems, these phenomena are results not only on the effect of TM doping but also on defects, especially oxygen vacancies (V_O). Oxygen vacancies have been proposed to play an important role in

the magnetic origin for O-DMSs. However, the origin of ferromagnetism in O-DMSs is due to the segregation of metallic clusters.

Recently, TM-doped CeO₂ has been also reported to exhibit ferromagnetism at and above room temperature [5-11]. Unlike other O-DMSs, CeO₂ has a cubic structure with lattice parameter $a = 0.54113$ nm [12] that will facilitate the integration of spintronic devices with advanced silicon microelectronic devices. The CeO₂ is often used as oxygen storage media due to its oxygen storage capacity via Ce⁴⁺/Ce³⁺ redox cycles [13-15]. Early work on CeO₂-based O-DMSs was focused on thin films [5-7] and only a little work has been carried out on powders, bulk, and nanocrystalline form [10-12,16]. Tiwari *et al.* [5] first discovered RT-FM in Ce_{1-x}Co_xO_{2-δ} (x ≤ 0.05) films deposited on a LaAlO₃ (001) substrate by a pulsed laser deposition (PLD) technique. These

¹Department of Physics, Faculty of Science, Khon Kaen University, Khon Kaen, 40002 Thailand

²School of Physics, Institute of Science, Suranaree University of Technology, Nakhon Ratchasima, 30000 Thailand

*Corresponding author. E-mail: santimaensiri@g.sut.ac.th; santimaensiri@gmail.com

films are transparent in a visible regime and exhibit a very high Curie temperature (T_C) ~ 740 - 875 K with large magnetic moments of $6.1 \pm 0.2 \sim 8.2 \pm 0.2 \mu_B/\text{Co}$. Following the work of Tiwari *et al.* and Song *et al.* [6] reported successful fabrication of $\text{Ce}_{1-x}\text{Co}_x\text{O}_{2-\delta}$ ($x = 0.03$) thin films with (111) preferential orientation deposited on a Si (111) substrate by PLD technique. Their deposited films show RT-FM with large magnetic moment of $5.8 \mu_B/\text{Co}$ and coercivity of 560 Oe. The authors also showed that the films could be deposited on glass but with smaller magnetic moment and coercivity. These results suggested that the FM in Co-doped CeO_2 depend not only on the doping concentration of transition element but also on the microstructure of film, including its crystallization, defects, vacancies, etc.. Vodungbo *et al.* [7] also reported FM in Co-doped CeO_2 thin films grown by PLD on SrTiO_3 and Si substrate. The films were ferromagnetic with a T_C above 400 K. These authors found that the amount of structural defects had a little effect on FM but the presence of oxygen during the growth or annealing reduced the FM drastically, suggesting that V_O played an important role in the magnetic coupling between Co ions. While Wen *et al.* [10] reported the ferromagnetism observed in undoped and Co-doped CeO_2 powders. The RT-FM in undoped CeO_2 originated from V_O while a slight Co doping in CeO_2 caused a nearly two orders enhancement of saturation magnetization (M_s) to 0.47 emu/g compared with the undoped sample. The author suggested that the large RT-FM observed in Co-doped CeO_2 powder originated from a combination effect of V_O and Co doping. Similarly, Ou *et al.* [11] reported RT-FM for $\text{Ce}_{1-x}\text{Co}_x\text{O}_2$ ($0 < x < 0.10$) nanorods prepared by electrodeposition route. The nanorods were ferromagnetic with a high T_C about 870 K and the largest M_s of 0.015 emu/g. They suggested that the RT-FM observed in Co-doped CeO_2 nanorods adjusted by the structural defects including V_O . The same behavior was found in nanoparticles of Fe-doped CeO_2 [12] with a M_s value of 0.0062 emu/g in 3 at. % Fe prepared by a sol-gel method, and Fe-doped CeO_2 [16] with a M_s value of 0.10 emu/g in 1 at. % Fe prepared by the proteic sol-gel process. The authors suggested that the RT-FM originated from exchange of F -center, which involved a combination of V_O and TM doping. However, the source of the magnetism is not only from the magnetically ordered spin of 3D dopants but also from the defects at surface. Ferromagnetic behaviors with large moments were also observed even in undoped CeO_2 [17] and CeO_2 doped with rare earth such as Nd, Sm [18] or Pr [19]. The authors suggested that defects play an important role in the magnetism, and that only a small fraction of the volume, possibly associated with the surface is active [17-20].

However, magnetic properties of nanospheres of Fe-doped CeO_2 have not yet been reported. In this

work, we report the ferromagnetism observed in Fe-doped CeO_2 nanospheres with particle size of ~ 100 - 200 nm synthesized by hydrothermal treatment using polyvinylpyrrolidone (PVP) as a surfactant. The crystallinity and morphology of these samples were characterized by XRD, Raman, and TEM. The valence states of Ce ions and Fe ions were also investigated by XANES, and the magnetic properties of the nanospheres were determined using VSM. The origin of RT-FM in this pure and Fe-doped CeO_2 system is also discussed.

Experimental

In the preparation of monodisperse Fe-doped CeO_2 spheres, one gram of PVP was mixed with 40 mL of de-ionized water at room temperature (27°C) until a homogeneous solution was obtained. Subsequently, 3 mmol of $\text{Ce}(\text{NO}_3)_3 \cdot 6\text{H}_2\text{O}$ (99.99%, Kanto) and $\text{Fe}(\text{NO}_3)_3 \cdot 9\text{H}_2\text{O}$ (99.9%, Kanto) were slowly added to the PVP solution to obtain a well-dissolved solution. The homogeneous solution was then transferred into a Teflon-lined stainless steel autoclave of 50 mL capacity and prepared at 200°C for 12 h. After the autoclave was cooled naturally to room temperature, the precipitate was collected and washed several times with distilled water. The final product was then dried overnight in a vacuum at 80°C . The same procedures were also applied for the preparation of undoped monodisperse CeO_2 spheres.

The prepared samples were characterized using XRD, Raman, TEM, XANES, and VSM. A Philips X-ray diffractometer with Cu $K\alpha$ radiation ($\lambda = 0.15406$ nm) was used to study the phases of the undoped CeO_2 and Fe-doped CeO_2 samples. Raman spectra were recorded at room temperature using a triple spectrometer (Jobin Yvon/Atago-Bussan T-64000, France). Morphology of the samples was obtained from transmission electron microscopy (TEM, JEOL JEM 2010 200 kV, Japan). High-resolution transmission electron microscopy (HRTEM) was performed using a JEOL JEM 2010 (300 kV, Japan). The Ce L_3 edge and Fe K edge XANES spectra were studied using X-ray absorption near-edge structure in transmission mode at the BL8 Station at Siam Photon Laboratory (Synchrotron Light Research Institute (Public Organization), SLRI) in Nakhon Ratchasima, Thailand. The magnetic measurements were performed at room temperature using a vibrating sample magnetometer (VSM 7403, Lakeshore, USA). The magnetic measurements were also performed using quantum design magnetometry (MPMS XL-7, USA) in the zero-field cooling (ZFC) and field cooling (FC) modes with an applied field of 1000 Oe.

Results and Discussion

XRD analysis

Figure 1 shows the XRD patterns of the undoped CeO₂ and Fe-doped CeO₂ prepared at 200°C for 12 h. All the samples exhibited peaks consistent with the face-centered cubic fluorite structure of CeO₂ in the standard data from JCPDS 34-0394 (vertical lines below the patterns). The XRD patterns of the Fe-doped CeO₂ are the same as that of undoped CeO₂, indicating that Fe ions might have been substituted into the CeO₂ lattice, and there are no secondary phases (such as FeO, Fe₂O₃, or Fe₃O₄) in these samples. The average crystallite sizes of all samples were calculated from X-ray line broadening of the peaks at (111), (200), (220), and (311) planes using Scherrer's equation. There was effect on the sizes of the crystallites with Fe doping (as listed in Table 1). The values of the lattice parameter *a* of all the samples calculated from the XRD spectra are shown in Table 1. The lattice parameter changed in comparison with undoped CeO₂. This change is possibly due to the replacement of larger Ce⁴⁺ (0.92 Å) by smaller Fe³⁺ (0.65 Å) or Fe²⁺ (0.78 Å), introducing

Ce³⁺ into the crystal lattice. Ce³⁺ have a higher ionic radius (1.034 Å) compared to Ce⁴⁺, and these ions introduce V_O. It is observed that CeO₂ and Fe-doped CeO₂ nanoparticles experience considerable lattice distortion, which is in good agreement with earlier reports [9,13,21]. Those reports indicated that doping causes a change in the Ce-O bond length (lattice distortion) and the overall lattice parameter.

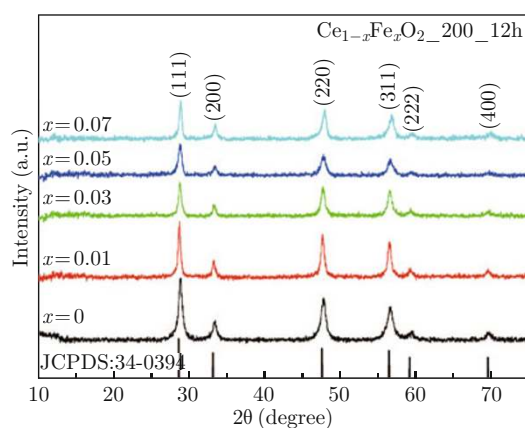


Fig. 1 XRD patterns of undoped CeO₂ and Fe-doped CeO₂ nanospheres prepared at 200°C for 12 h.

Table 1 Summary of crystallite sizes from XRD, Lattice constant, and Magnetization (*M*) of undoped CeO₂ and Fe-doped CeO₂ nanospheres prepared at 200°C for 12 h

Sample Ce _{1-x} Fe _x O ₂	Crystallite size (nm)	Lattice constant, <i>a</i> (nm)	Peak area	Percentage of Ce ³⁺ (%)	<i>M</i> at 10 kOe (emu/g)
<i>x</i> = 0	19.6	0.5420 ± 0.0003	5.884 (Ce ⁴⁺) 6.095 (Ce ⁴⁺) 1.289 (Ce ³⁺)	9.7	0.0026
<i>x</i> = 0.01	18.1	0.5423 ± 0.0012	-	-	0.0018
<i>x</i> = 0.03	15.2	0.5427 ± 0.0015	-	-	0.0058
<i>x</i> = 0.05	12.7	0.5414 ± 0.0018	3.160 (Ce ⁴⁺) 2.304 (Ce ⁴⁺) 1.000 (Ce ³⁺)	15.5	0.032
<i>x</i> = 0.07	14.8	0.5406 ± 0.0018	-	-	0.027

Raman analysis

The formation of a cubic structure in the Fe-doped CeO₂ nanospheres was further supported by Raman spectra. Figure 2 shows typical spectra of Fe-doped CeO₂. The peak at about 443-463 cm⁻¹ can be assigned to the F_{2g} mode of CeO₂, which is the characteristic mode of the Ce-O8 vibrational unit [12]. While the peaks at about 600 cm⁻¹ can be assigned to intrinsic V_O (marked with Δ in Fig. 2), which is sensitive to any disorder in the oxygen sublattice resulting from thermal, doping, or grain size [22-25]. The intensity of intrinsic V_O Raman active mode in Ce_{1-x}Fe_xO₂ samples is pronounced than in pure CeO₂ samples. Such behavior confirms our previous statement that incorpo-

ration of Fe ions in CeO₂ lattice can be attributed to more V_O, especially at *x* = 0.2. In the Raman spectrum of Ce_{1-x}Fe_xO₂ nanospheres, the F_{2g} mode is shifted to lower energies with increasing Fe content, which exhibits redshift in this mode [26]. The energy shows redshift of 2, 12, 16, and 19 cm⁻¹ for samples with Fe contents of 0.01, 0.03, 0.05, and 0.07, respectively, compared to that of the pure CeO₂ nanospheres. This behavior shows the electron molecular vibrational coupling due to increased concentration of substitution of Fe ions in the Ce lattice and the introduction of V_O. Beside the F_{2g} and V_O modes, a weak band appears at 210, 277 and 394 cm⁻¹ (marked with □ in Fig. 2) observed in Ce_{1-x}Fe_xO₂ (*x* = 0.2), which is assigned to hematite (α-Fe₂O₃) structure. The appearance of

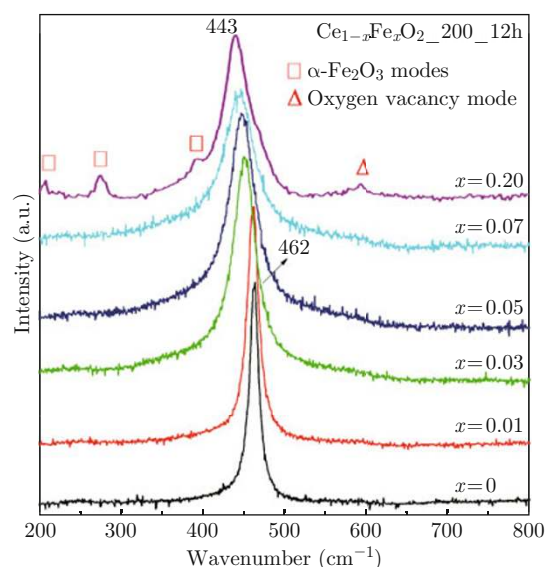


Fig. 2 Raman spectra of undoped CeO_2 and Fe-doped CeO_2 nanospheres prepared at 200°C for 12 h.

modes characteristic for hematite structures can be a consequence of impurity phase, implying a possible substitution limit for Fe ions in CeO_2 .

TEM analysis

The morphology and structure of Fe-doped CeO_2 samples were investigated by TEM as shown in Fig. 3(a)-(e). The TEM bright field images show that the products contain monodisperse nanospheres with a diameter of $100\sim 200$ nm. The average particle size obtained from TEM is larger than the crystallite size obtained from the XRD patterns. This result is similar to the work reported by Zhou *et al.* [27] in which spherical CeO_2 crystallites assembled by nanoparticles were formed during hydrothermal treatment, because small nanoparticles of CeO_2 aggregated, and gradually evolved into a spherical assemblage to achieve a low surface energy, as shown in Fig. 4. From Fig. 3(b)-(e),

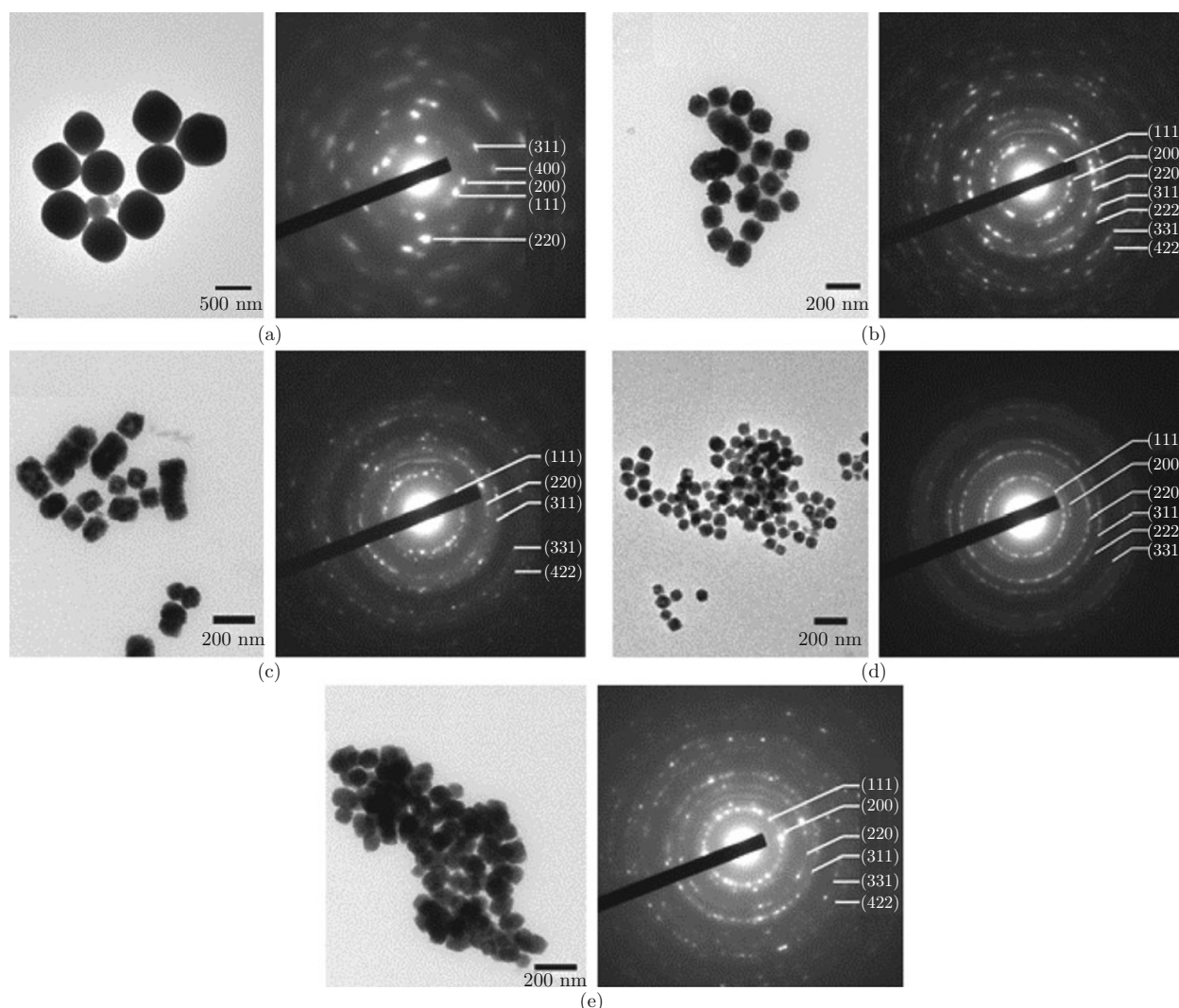


Fig. 3 TEM bright field images with corresponding selected-area electron diffraction (SAED) patterns of Fe-doped CeO_2 nanospheres prepared at 200°C for 12 h for (a) $x = 0$, (b) $x = 0.01$, (c) $x = 0.03$, (d) $x = 0.05$ and (e) $x = 0.07$.

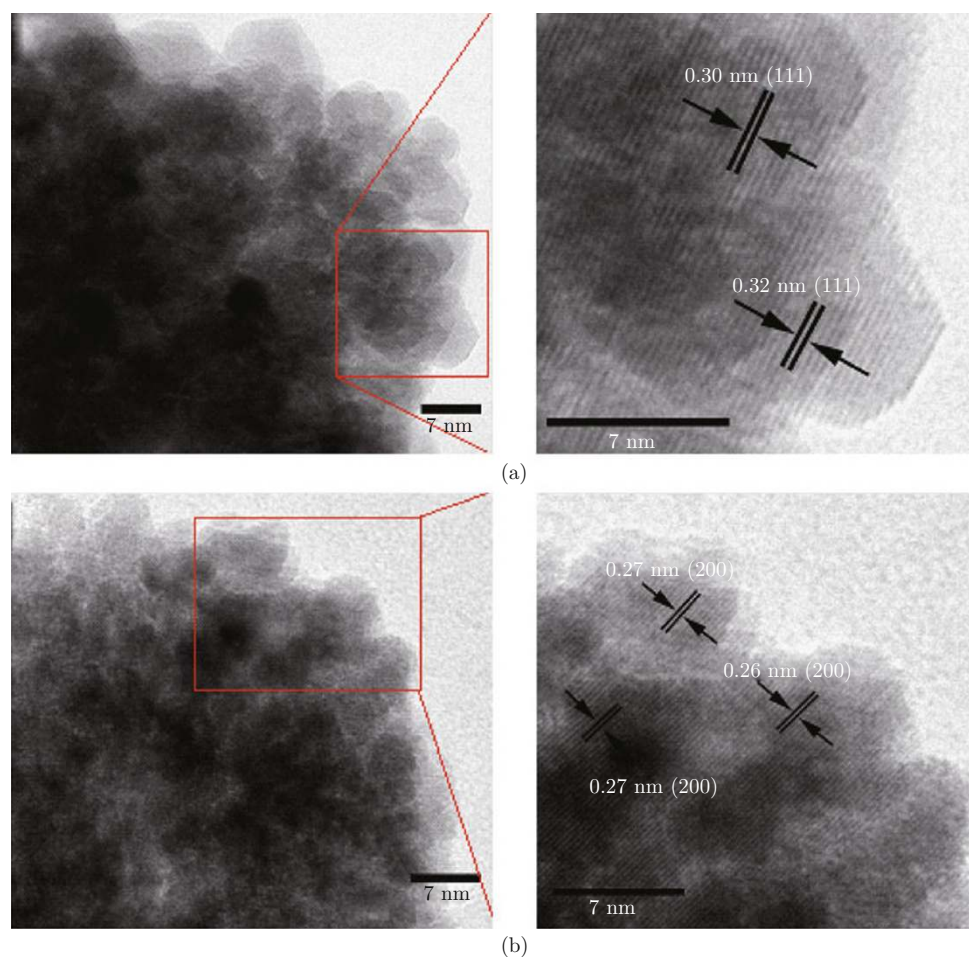


Fig. 4 HRTEM images of Fe-doped CeO_2 nanospheres prepared at 200°C for 12 h for (a) $x = 0.03$, and (b) $x = 0.05$.

morphologies of Fe-doped CeO_2 clearly show that nanospheres become smaller as the doped Fe content increases, which agree with the XRD results. It is possible that doping Fe^{3+} can forbid the crystal growth. With higher concentrations of Fe^{3+} , it would possibly increase the blockade of crystal growth, giving rise to a decrease in particle size. The same behavior was found in nanoparticles of TiO_2 that prohibit the growth in [001] direction after Fe doping as reported by Wen *et al.* [28]. They reported that Fe^{3+} on the surface can form effective pathways for charge interfacial transfer for increasing the photocatalytic activity of TiO_2 . As a result of this, Fe^{3+} are on the surface of spherical aggregates due to the small particle size, which is beneficial for increasing the magnetic interaction of Fe-doped CeO_2 nanospheres. The corresponding selected area electron diffraction (SAED) patterns of the products show spotty ring patterns indicative of a face-centered cubic structure of CeO_2 (JCPDS: 34-0394), which is in agreement with the XRD results. HRTEM images of $\text{Ce}_{1-x}\text{Fe}_x\text{O}_2$ for $x = 0.03$ and 0.05 , are shown in Fig. 4(a) and 4(b), respectively. The d spacings of the lattice fringes of ~ 0.30 and 0.32 nm (Fig. 4(a)) calculated from the HRTEM images are corresponding to the

(111) plane of CeO_2 . Similarly, the d spacings of ~ 0.26 and 0.27 nm (Fig. 4(b)) calculated from the HRTEM images match with (200) plane of CeO_2 . These are in agreement with the standard data (JCPDS: 34-0394). This result confirms the formation mechanism of Fe-doped CeO_2 nanoparticles into nanospheres.

XANES analysis

The valence state of Ce in undoped CeO_2 and Fe-doped CeO_2 nanospheres and valence state of Fe were determined by XANES. The XANES spectra at Ce L_3 edge were measured in transmission mode, and the Fe K edge XANES spectra of the samples were measured in Fluorescent mode at RT at the BL8 station. Figure 5(a) shows the edge energies of the CeCl_3 (Ce^{3+}) standard, CeO_2 (Ce^{4+}) standard, pure CeO_2 sample, and $\text{Ce}_{1-x}\text{Fe}_x\text{O}_2$ ($x = 0.05$) sample for comparison. The standard CeCl_3 has a single peak illustrated by one intense white line at approximately 5728.8 eV due to the dipole-allowed transition of Ce $2p$ to Ce $4f^15d_{e_g}\underline{L}$ final states (represented with $2p4f^15d_{e_g}\underline{L}$, where \underline{L} denotes an oxygen ligand $2p$ hole); this characterizes the Ce in the Ce^{3+} valence state. In the standard CeO_2 , all the

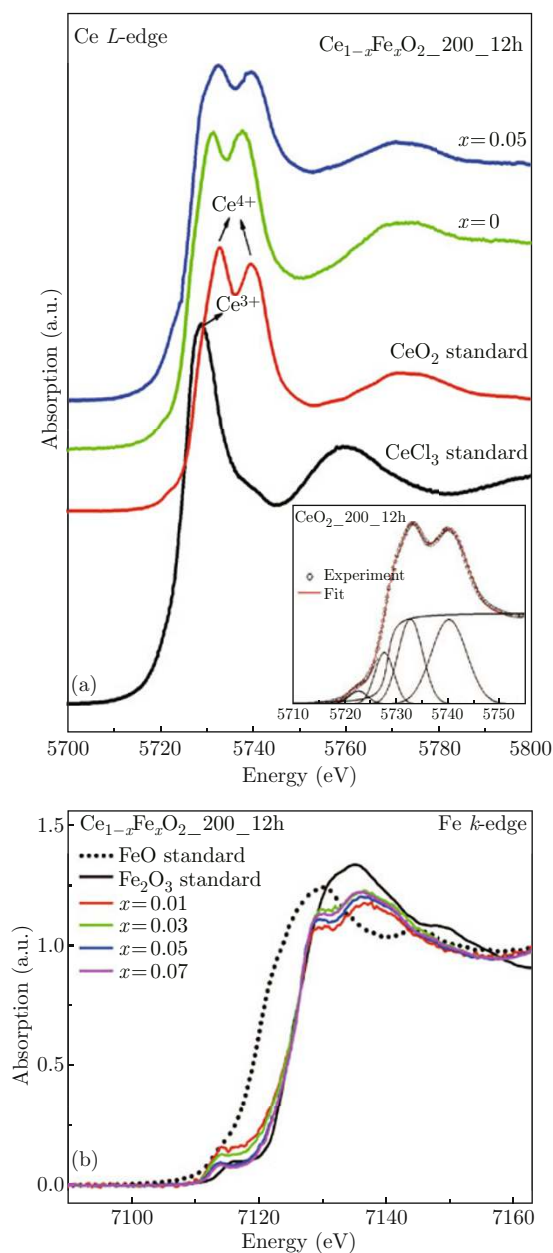


Fig. 5 (a) XANES spectra at the Ce L_3 absorption edge for CeCl_3 , CeO_2 standard, and XANES spectra of samples $x = 0$, and $x = 0.05$ at 200°C for 12 h (Inset shows Gaussian fits of XANES spectra of Ce for samples $x = 0$); (b) XANES spectra at the Fe K absorption edge for FeO (Fe^{2+}) standard, Fe_2O_3 (Fe^{3+}) standard, and XANES spectra of Fe-doped CeO_2 nanospheres at 200°C for 12 h.

spectra are shifted to higher energies, and the white line is split into two peaks with nearly the same intensities at approximately 5732.8 and 5739.8 eV due to an electron excited from Ce 2p to Ce $4f^15d_{g\bar{L}}$ final states (represented with $2p4f^15d_{g\bar{L}}$) and the excited electron in Ce 4f state and Ce 2p to Ce $4f^05d$ final states (represented with $2p4f^05d$), no electron in the 4f state, respectively, corresponding to the Ce^{4+} valence state [29]. At low energy, the peak of the standard CeO_2 is a pre-edge peak, which is assigned to final states of $2p5d$ with

delocalized d character at the bottom of the conduction band [30, 31]. The three Ce peak positions of all the samples are close to the values of the CeCl_3 and CeO_2 standards. This result indicates that the Ce ions in our samples are in a mixed valence state of Ce^{3+} and Ce^{4+} . The quantitative analysis of the valence state of Ce in each of the three states of Fe-doped CeO_2 nanospheres was performed using multi-peak Gaussian fitting obtained from the XANES spectra [32], as shown in inset of Fig. 5(a). The distribution of Ce^{3+} and Ce^{4+} can be obtained by calculation the area ratio of Ce^{3+} and Ce^{4+} . The relative concentration of Ce^{3+} are $\sim 9.7\%$ and $\sim 15.5\%$ for undoped CeO_2 and Fe-doped CeO_2 samples ($x = 0.05$), respectively. It was observed that the percentage of Ce^{3+} of the $\text{Ce}_{1-x}\text{Fe}_x\text{O}_2$ samples ($x = 0.05$) is higher than those of undoped CeO_2 samples because of the incorporation of Fe. The percentage of Ce^{3+} is $\sim 15.5\%$ in Fe doped, which is lower than those of 21.5% in the $\text{Ce}_{1-x}\text{Fe}_x\text{O}_2$ samples ($x = 0.1$) reported by Wang *et al.* [33] Their result was calculated based on X-ray photoelectron spectroscopy (XPS), which more sensitive to surface.

Figure 5(b) shows the edge energies of the FeO (Fe^{2+}) standard, Fe_2O_3 (Fe^{3+}) standard, and Fe-doped CeO_2 samples at different concentrations prepared at 200°C for 12 h for comparison. The shift of the edge position can be used to determine the valence state. From Fig. 5(b), edge position of FeO (Fe^{2+}) standard is approximately 7120 eV, while Fe_2O_3 (Fe^{3+}) standard is approximately 7125 eV. These can be used simply as a fingerprint of phases and valence state. It is seen that the edge positions of all the samples were quite similar to those of the Fe_2O_3 standard at approximately 7125 eV. In addition, the feature of all samples was very similar in terms of shape and position to the Fe_2O_3 standard at approximately 7128 and 7134 eV, respectively. Thus, this result indicates that most of the Fe ions in our samples are in the Fe^{3+} valence state. These spectra at the Fe K edge are very similar to those of the Fe from aerosols samples reported by Ohta *et al.* [34] showing a pre-edge feature approximately 7114 eV due to an electron excited from the Fe 1s to the Fe 3D final states.

Magnetic properties

Figure 6 shows the field dependence of the specific magnetization (M - H curve) of undoped CeO_2 and Fe-doped CeO_2 samples, obtained from VSM measurements at RT. The magnetic component corresponding to the samples holder was subtracted from all the presented data. The samples show weak RT-FM and the M_S increases with increasing Fe concentration. The highest M_S was observed for $x = 0.05$ with value of approximately 0.03 emu/g at 10 kOe. The magnetizations of the Fe-doped CeO_2 samples for $x = 0.07$ have both FM and paramagnetism (PM) increasing with an

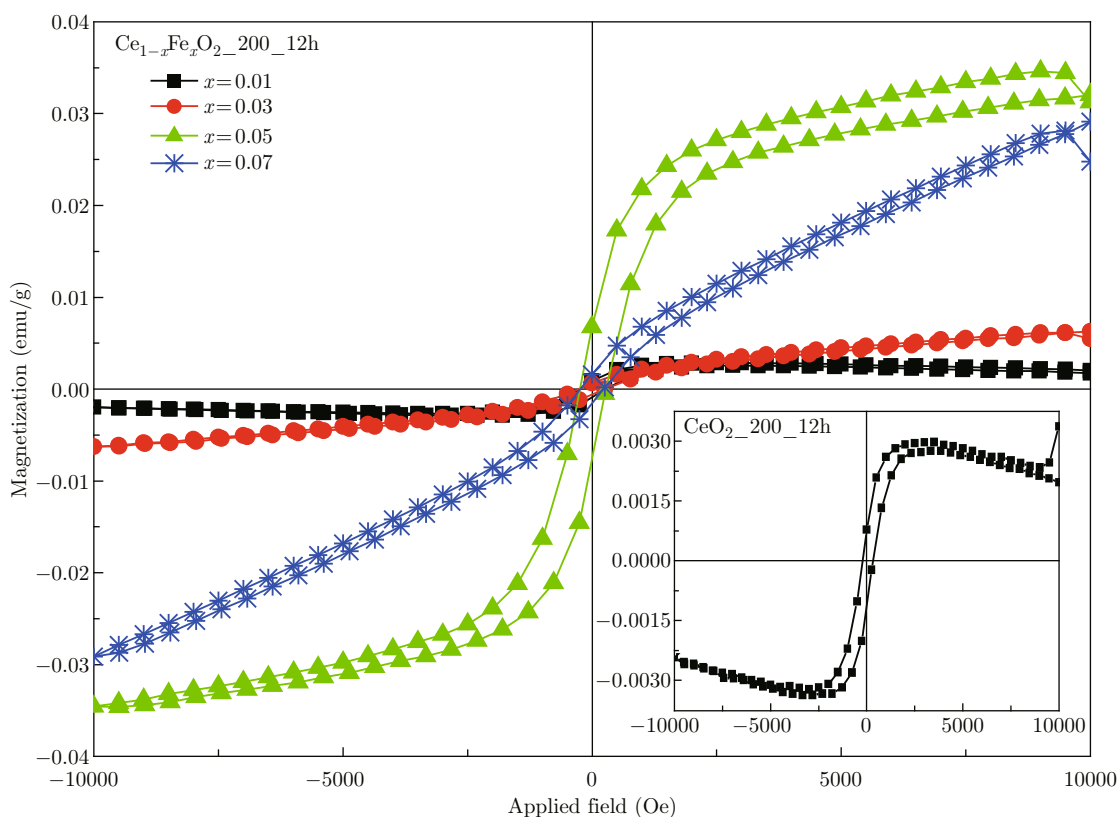


Fig. 6 Magnetic properties of Fe-doped CeO₂ nanospheres prepared at 200°C for 12 h (inset shows magnetic loop of undoped CeO₂).

increasing magnetic field. The M values of all the samples are shown in Table 1. In comparison to other works, the M_S value of 0.03 emu/g in this work is lower than the reported M_S values for Fe-doped CeO₂ powders at $x = 0.01$ (0.1 emu/g at 45 kOe) [12] and Fe-doped CeO₂ pellets at $x = 0.05$ (0.24 emu/g at 10 kOe) [35]. However, the M_S value in our result is higher than those of other reports, i.e., Fe-doped CeO₂ nanocrystals at $x = 0.03$ (0.0062 emu/g at 10 kOe) [16] and Fe-doped CeO₂ nanocrystals at $x = 0.12$ (0.02 emu/g at 0.6 kOe) [26]. The difference in M_S in the magnetic properties of Fe-doped CeO₂ materials depends on the preparation conditions such as temperature and atmosphere [36,37]. We also observed RT-FM in undoped CeO₂ nanospheres with M_S of approximately 0.0026 emu/g at 10 kOe. This result is interesting because bulk CeO₂ is an insulator with Ce⁴⁺ in the 4f⁰ configuration. Generally, magnetic ordering in insulating oxides is antiferromagnetic ordering due to the superexchange coupling, but CeO₂ is often used as a storage medium because a V_O can easily be formed in CeO₂. Similar results have been obtained in some other work [17,21]. Sundaresan *et al.* [21] reported that the weak ferromagnetism, with M_S of approximately 0.0019 emu/g at 5 kOe in pure CeO₂ nanoparticles (average size of 15 nm) as well as in other undoped oxide semiconductors, results from the exchange interactions between electron

spin moment of Ce³⁺ and the V_O at the particle surface. This direct ferromagnetic coupling is called the F -center exchange (FCE) [13,38,40]. It is possible that V_O can create magnetic moments on neighboring Ce ions of Ce³⁺-∇-Ce³⁺, where ∇ denotes a V_O.

For explanation the origin of the ferromagnetic contribution in Fe ions-doped CeO₂ nanospheres, the following arguments are proposed. First, the ferromagnetic behavior is associated with FCE coupling, in which both V_O and Fe ions are involved. In this work, the XANES spectra show evidence of Fe³⁺ substitution in CeO₂, and the Ce ions of 3+ state (with 4f¹ configuration), which can be attributed to V_O in Fe-doped CeO₂ samples. Therefore, the RT-FM in these samples was suggested according to the FCE of Fe³⁺-∇-Fe³⁺ complex in the structure. This FCE forms bound magnetic polarons (BMP) and neighboring BMPs can overlap and result in the long-range Fe-Fe ferromagnetic coupling in CeO₂. The radius of the electron trapped orbital, that overlaps the d shells of both Fe ion neighbors, is of the order $a_0\varepsilon$, where a_0 is the Bohr radius, and ε is the dielectric constant of the material. In CeO₂ ($\varepsilon = 26$), the radius of the F -electron orbital is estimated to be ~ 14 Å [5], which is required for a long-range FM order. As Fe³⁺ (3D⁵) ions in the case of low-spin state only have unoccupied minority spin orbitals [40], the trapped electron in vacancy will be ↓

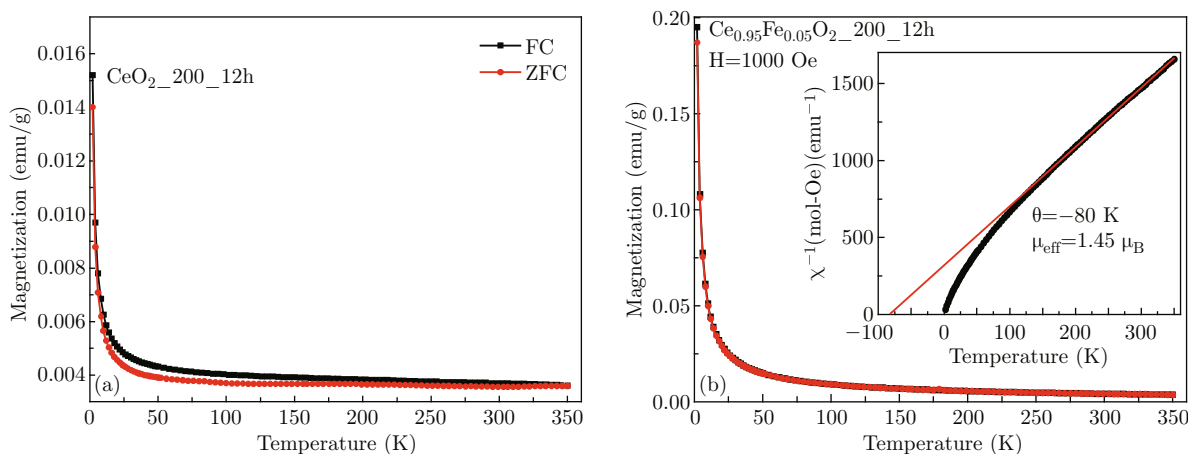


Fig. 7 M - T curves at 1 kOe of samples nanospheres prepared at 200°C for 12 h (a) Undoped CeO_2 and (b) Fe-doped CeO_2 ($x = 0.05$). Inset exhibits the Curie-Weiss behavior of the inverse susceptibility for Fe-doped CeO_2 ($x = 0.05$).

and the two Fe neighbors \uparrow , according to the Hund's rule and Pauli Exclusion Principle. Second, the double exchange interaction is investigated. It is coupling between nearest neighbor of Fe ions with different valence and oxygen ions ($\text{Fe}^{2+}\text{-O}^{2-}\text{-Fe}^{3+}$). However, mechanism of ferromagnetism on this interaction cannot produce long-range magnetic order because of concentrations of Fe ions of a few percent in structure. Moreover, the XANES results in Fe-doped CeO_2 showed that no mixed of Fe ions exist. Finally, ferromagnetism may originated by Fe clusters. If Fe cluster exist the magnetic moment would be proportional to the amount of Fe concentration but no tendency in our M results observed. Therefore, the RT-FM in these samples, and the exchange interaction between Vo and the surrounding of Fe^{3+} was suggested as being a result of the FM according to the FCE.

It is observed that the loss of M induced by Fe-doped at $x = 0.01$ compared to undoped CeO_2 . This case is due to the pairing of the electron clouds surrounding V_O , which are electron excess left behind in the vacancies [41]. With high concentrations of Fe ions, it would possibly increase the amount of magnetic moments and enhance significantly in ferromagnetism. Moreover, the additional exchange interactions between the spins of the Ce^{3+} are responsible for the observed enhanced ferromagnetism in these samples. At higher Fe concentrations ($x = 0.07$) in our case, Fe ions become closer together as the Fe content increases, which increases the superexchange interactions between these neighboring Fe ions of $\text{Fe}^{3+}\text{-O}^{2-}\text{-Fe}^{3+}$ gives rise to an antiferromagnetic behavior. As a result of this, the ferromagnetism decreases in the average magnetic moment per Fe ion and appears to be a paramagnetic effect. However, the exact mechanism for different magnetizations of Fe-doped CeO_2 samples with different Fe concentrations is still unclear, and further work is needed.

The temperature dependence of magnetization (M –

T curve) of undoped CeO_2 and Fe-doped CeO_2 ($x = 0.05$) samples were measured under H of 1 kOe in the zero field cooling (ZFC) and field cooling (FC) modes as shown in Fig. 7. The ZFC-FC curves showed similar behavior of each sample and no evidence of secondary phase was existed down to 2 K. The T_c or Neel temperatures (T_N) in these samples do not match to those values of Fe ($T_C \sim 1043$ K), FeO ($T_N \sim 200$ K), $\alpha\text{-Fe}_2\text{O}_3$ ($T_C \sim 240$ K), or Fe_3O_4 ($T_C \sim 858$ K) [42]. From PM component in Fe-doped CeO_2 samples, the paramagnetic region can be well fitted using a simple Curie-Weiss equation, $\chi = C/(T-\theta)$ where χ is susceptibility, C is the Curie constant, T and θ are experimental temperature and the Curie-Weiss temperature, respectively. The linear plot of inverse χ dependence of the temperature is shown in the inset of Fig. 7(b). It exhibited a good fit obtained at high temperature for Fe-doped CeO_2 samples, except in undoped CeO_2 . The sample had a negative value of θ (~ -80 K), which indicates antiferromagnetic interactions between Fe ions. This behavior can be described using the Curie-Weiss equation with the effective magnetic moments of $\mu_{eff} \approx 1.45 \mu_B$ for Fe-doped CeO_2 . This is close to that of the low-spin state of Fe^{3+} ion ($\mu_{eff} = 1.73 \mu_B$). These effective magnetic moments correspond to the free Fe^{3+} without magnetic interactions or PM defect in the system.

Conclusions

Nanospheres of undoped CeO_2 and Fe-doped CeO_2 have been successfully synthesized by a hydrothermal method using PVP as a surfactant. The XRD and SEAD results indicated that all the samples had a face-centered cubic structure and that no secondary phase was detected, which indicated that Fe^{3+} ions were substituted in Ce^{4+} sites. Fe^{3+} doping causes redshift of

the F_{2g} Raman mode due to the increased concentration of Ce^{3+} with oxygen vacancies. The oxygen vacancy is confirmed by XANES measurements, which reveals that most of the Fe ions are in the 3+ state, and that some Ce ions transform to the 3+ state. The Ce^{3+} and Fe^{3+} spin electrons are induced weak RT-FM. This behavior indicated that the ferromagnetism is essentially related to oxygen vacancy/defects.

Acknowledgements

The authors would like to thank the Synchrotron Light Research Institute (Public Organization), Nakhon Ratchasima, Thailand for XANES facilities, and Clarendon Laboratory, Department of Physics, University of Oxford, United Kingdom for quantum design magnetometry facilities. S. Phokha would like to acknowledge the financial support for her Ph.D. studies from the Thailand Research Fund through the Royal Golden Jubilee Ph.D. program (Grant No. PHD/0275/2550). This work was supported by Suranaree University of Technology (SUT) and by the Office of the Higher Education Commission under NRU project of Thailand.

References

- [1] T. Dietl, H. Ohno, F. Matsukura, J. Cibert and D. Ferrand, "Zener model description of ferromagnetism in zinc-blende magnetic semiconductors", *Science* 287(5455), 1019-1022 (2000). <http://dx.doi.org/10.1126/science.287.5455.1019>
- [2] S. J. Pearton, W. H. Heo, M. Ivill, D. P. Norton and T. Steiner, "Dilute magnetic semiconducting oxides", *Semicond. Sci. Technol.* 19(10), R59 (2004). <http://dx.doi.org/10.1088/0268-1242/19/10/R01>
- [3] N. H. Hong, J. Sakai, N. Poirot and V. Brize, "Room-temperature ferromagnetism observed in undoped semiconducting and insulating oxide thin films", *Phys. Rev. B* 73(13), 132404 (2006). <http://dx.doi.org/10.1103/PhysRevB.73.132404>
- [4] X. Chen, G. Li, Y. Su, X. Qui, L. Li and Z. Zou, "Synthesis and room-temperature ferromagnetism of CeO_2 nanocrystals with nonmagnetic Ca^{2+} doping", *Nanotechnology* 20(11), 115606 (2009). <http://dx.doi.org/10.1088/0957-4484/20/11/115606>
- [5] A. Tiwari, V. M. Bhosle, S. Ramachandran, N. Sudhakar, J. Narayan, S. Budak and A. Gupta, "Ferromagnetism in Co doped CeO_2 : Observation of a giant magnetic moment with a high Curie temperature", *Appl. Phys. Lett.* 88(14), 142511 (2006). <http://dx.doi.org/10.1063/1.2193431>
- [6] Y. Q. Song, H. W. Zhang, Q. Y. Wen, Y. X. Li and J. Q. Xiao, "Room-temperature ferromagnetism of co-doped CeO_2 thin films on si(111) substrates", *Chin. Phys. Lett.* 24(1), 218-221 (2007). <http://dx.doi.org/10.1088/0256-307X/24/1/059>
- [7] B. Vodungbo, Y. Zheng, F. Vidal, D. Demaille, V. H. Etgens and D. H. Mosca, "Room temperature ferromagnetism of Co doped $CeO_{2-\delta}$ diluted magnetic oxide: Effect of oxygen and anisotropy", *Appl. Phys. Lett.* 90(6), 062510 (2007). <http://dx.doi.org/10.1063/1.2472520>
- [8] V. Fernandes, J. J. Klein, N. Mattoso, D. H. Mosca, E. Silveira, E. Ribeiro, W. H. Schreiner, J. Varalda and A. J. A. de Oliveira, "Room temperature ferromagnetism in Co-doped CeO_2 films on Si(001)", *Phys. Rev. B* 75(12), 121304R (2007). <http://dx.doi.org/10.1103/PhysRevB.75.121304>
- [9] A. Thurber, K. M. Reddy, V. Shutthanandan, M. H. Engelhard, C. Wang, J. Hays and Punnoose, "Ferromagnetism in chemically synthesized CeO_2 nanoparticles by Ni doping", *Phys. Rev. B* 76(16), 165206 (2007). <http://dx.doi.org/10.1103/PhysRevB.76.165206>
- [10] Q. Y. Wen, H. W. Zhang, Y. Q. Song, Q. H. Yang, H. Zhu and J. Q. Xiao, "Room-temperature ferromagnetism in pure and Co doped CeO_2 powders", *J. Phys.: Condens. Mat.* 19(24), 246205 (2007). <http://dx.doi.org/10.1088/0953-8984/19/24/246205>
- [11] Y. N. Ou, G. R. Li, J. H. Liang, Z. P. Feng and Y. X. Tong, " $Ce_{1-x}Co_xO_{2-\delta}$ nanorods grown by electrochemical deposition and their magnetic properties", *J. Phys. Chem. C* 114(32), 13509-13514 (2010). <http://dx.doi.org/10.1021/jp1038128>
- [12] P. C. A. Brito, D. A. A. Santos, J. G. S. Duque and M. A. M. Macedo, "Structural and magnetic study of Fe-doped CeO_2 ", *Physica B* 405(7), 1821-1825 (2010). <http://dx.doi.org/10.1016/j.physb.2010.01.054>
- [13] M. Y. Ge, H. Wang, E. Z. Liu, H. F. Liu, J. Z. Jiang, Y. K. Li, Z. A. Xu and H. Y. Li, "On the origin of ferromagnetism in CeO_2 nanocubes", *Appl. Phys. Lett.* 93, 062505 (2008). <http://dx.doi.org/10.1063/1.2972118>
- [14] S. Kumar, Y. J. Kim, B. H. Koo, and C. G. Lee and J. Nanosci. "Structural and magnetic properties of Ni doped CeO_2 nanoparticles", *J. Nanosci. Nanotechnol.* 10(11), 7204-7207 (2010). <http://dx.doi.org/10.1166/jnn.2010.2751>
- [15] P. O. Maksimchuk, A. A. Masalov, Yu.V. Malyukin, "Spectroscopically detected formation of oxygen vacancies in nano-crystalline CeO_{2-x} ", *J. Nano-Electron. Phys.* 5(1), 01004 (2013).
- [16] S. Maensiri, S. Phokha, P. Laokul, and S. Seraphin, "Room temperature ferromagnetism in Fe-doped CeO_2 nanoparticles", *J. Nanosci. Nanotechnol.* 9(11), 6415-6420 (2009). <http://dx.doi.org/10.1166/jnn.2009.1372>
- [17] S. Phokha, S. Pinitsoontorn, P. Chirawatkul, Y. Poo-arporn and S. Maensiri, "Synthesis, characterization, and magnetic properties of monodisperse CeO_2 nanospheres prepared by PVP-assisted hydrothermal method", *Nanoscale Res. Lett.* 7, 425 (2012). <http://dx.doi.org/10.1186/1556-276X-7-425>
- [18] M. C. Dimri, H. Khanduri, H. Kooskora, J. Subbi, I. Heinmaa, A. Mere, J. Krustok and R. Stern, "Ferro-

- magnetism in rare earth doped cerium oxide bulk samples”, *Phys. Status Solidi A* 209(2), 353-358 (2012). <http://dx.doi.org/10.1002/pssa.201127403>
- [19] N. Paunović Z. D. Mitrović R. Scurtu, S. Aškračić M. Prekajski, B. Matović and Z. V. Popović “Suppression of inherent ferromagnetism in Pr-doped CeO₂ nanocrystals”, *Nanoscale*, 4(17), 5469-5476 (2012). <http://dx.doi.org/10.1039/c2nr30799e>
- [20] K. Ackland, L. M. A. Monzon, M. Venkatesan and J. M. D. Coey, “Magnetism of Nanostructured CeO₂”, *IEEE Trans. Magn.* 47(10), 3509-3512 (2011). <http://dx.doi.org/10.1109/TMAG.2011.2150743>
- [21] A. Sundaresan, R. Bhargavi, N. Rangarajan, U. Sidsh and C. N. R. Rao, “Ferromagnetism as a universal feature of nanoparticles of the otherwise nonmagnetic oxides”, *Phys. Rev. B* 74(16), 161306(R) (2006).
- [22] S. Maensiri, C. Marsingboon, P. Loakul, W. Jareonboon, V. Promarak, P. L. Anderson and S. Seraphin, “Egg white synthesis and photoluminescence of plate-like clusters of CeO₂ nanoparticles”, *Cryst. Growth. Des.* 7(5), 950-955 (2007). <http://dx.doi.org/10.1021/cg0608864>
- [23] S. Phoka, P. Laokul, E. Swatsitang, V. Promarak, S. Seraphin and S. Maensiri, “Synthesis, structural and optical properties of CeO₂ nanoparticles synthesized by a simple polyvinyl pyrrolidone (PVP) solution route”, *Mater. Chem. Phys.* 115(1), 423-428 (2009). <http://dx.doi.org/10.1016/j.matchemphys.2008.12.031>
- [24] I. Kosacki, T. Suzuki, V. Petrovsky, H. U. Anderson and Ph. Colomban, “Raman scattering and lattice defects in nanocrystalline CeO₂ thin films”, *Solid State Ionics* 149(1-2), 99-105 (2002).
- [25] I. Kosacki, V. Petrovsky, H. U. Anderson and Ph. Colomban, “Raman spectroscopy of nanocrystalline ceria and zirconia thin films”, *J. Am. Ceram. Soc.* 85(11), 2646-2650 (2002). <http://dx.doi.org/10.1111/j.1151-2916.2002.tb00509.x>
- [26] Z. D. Dohcevic-Mitrovic, N. Paunovic, M. Radovic, Z. V. Popovic, B. Matovic, B. Cekic and V. Ivanovski, “Valence state dependent room-temperature ferromagnetism in Fe-doped ceria nanocrystals”, *Appl. Phys. Lett.* 96(20), 203104 (2010). <http://dx.doi.org/10.1063/1.3431581>
- [27] F. Zhou, X. Ni, Y. Zhang and H. Zheng, “Size-controlled synthesis and electrochemical characterization of spherical CeO₂ crystallites”, *J. Colloid Interf. Sci.* 307(1), 135-138 (2007). <http://dx.doi.org/10.1016/j.jcis.2006.11.005>
- [28] L. Wen, B. Liu, X. Zhao, K. Nakata, T. Murakami and A. Fujishima, “Synthesis, characterization, and photocatalysis of Fe-doped TiO₂: A combined experimental and theoretical study”, *Int. J. Photoenergy* 2012, 368750 (2012). <http://dx.doi.org/10.1155/2012/368750>
- [29] J. Hormes, M. Pantelouris, G.B. Balazs and B. Rambabu, “X-ray absorption near edge structure (XANES) measurements of ceria-based solid electrolytes”, *Solid State Ionics* 136-137, 945-954 (2000). [http://dx.doi.org/10.1016/S0167-2738\(00\)00533-6](http://dx.doi.org/10.1016/S0167-2738(00)00533-6)
- [30] F. Zhang, P. Wang, J. Koberstein, S. Khalid and S. W. Chan, “Cerium oxidation state in ceria nanoparticles studied with X-ray photoelectron spectroscopy and absorption near edge spectroscopy”, *Surf. Sci.* 563(1-3), 78-82 (2004). <http://dx.doi.org/10.1016/j.susc.2004.05.138>
- [31] J. Zhang, Z. Wu, T. Liu, T. Hu, Z. Wu and X. Ju, “XANES study on the valence transitions in cerium oxide nanoparticles”, *J. Synchrotron Radiat.* 8, 531-532 (2001). <http://dx.doi.org/10.1107/S0909049500016022>
- [32] C. Wan, X. Ju, Y. Qi, Y. Zhang, S. Wang, X. Liu and L. Jiang, “Synchrotron XRD and XANES studies of cerium-doped NaAlH₄: Elucidation of doping induced structure changes and electronic state”, *J. Alloy. Compd.* 481(1-2), 60-64 (2009). <http://dx.doi.org/10.1016/j.jallcom.2009.03.128>
- [33] J. Wang, B. Zhang, M. Shen, J. Wang, W. Wang, J. Ma, S. Liu and L. Jia, “Effects of Fe-doping of ceria-based materials on their microstructural and dynamic oxygen storage and release properties”, *J. Sol-Gel Sci. Techn.* 58(1), 259-268 (2011). <http://dx.doi.org/10.1007/s10971-010-2386-3>
- [34] A. Ohta, H. Tsuno, H. Kagi, Y. Kanai, M. Nomura, R. Zhang, S. Terashima and N. Imai, “Chemical compositions and XANES speciations of Fe, Mn and Zn from aerosols collected in China and Japan during dust events”, *Geochem. J.* 40(4), 363-376 (2006). <http://dx.doi.org/10.2343/geochemj.40.363>
- [35] R. K. Singhal, P. Kumari, S. Kumar, S. N. Dolia, Y. T. Xing, M. Alzamora, U. P. Deshpande, T. Shripathi and E. Saitovitch, “Room temperature ferromagnetism in pure and Co- and Fe-doped CeO₂ dilute magnetic oxide: Effect of oxygen vacancies and cation valence”, *J. Phys. D: Appl. Phys.* 44(16), 165002 (2011). <http://dx.doi.org/10.1088/0022-3727/44/16/165002>
- [36] S. Maensiri, S. Phokha, P. Laokul and S. Seraphin, “Room temperature ferromagnetism in Fe-Doped CeO₂ nanoparticles”, *J. Nanosci. Nanotechnology* 9(11), 6415-6420 (2009).
- [37] J. M. D. Coey, M. Venkatesan and C. B. Fitzgerald, “Donor impurity band exchange in dilute ferromagnetic oxides”, *Nat. Mater.* 4(2), 173-179 (2005). <http://dx.doi.org/10.1038/nmat1310>
- [38] V. Fernandes, R. J. O. Mossaneck, P. Schio, J. J. Klein, A. J. A. de Oliveira, W. A. Ortiz, N. Mattoso, J. Varalda, W. H. Schreiner, M. Abbate and D. H. Mosca, “Dilute-defect magnetism: Origin of magnetism in nanocrystalline CeO₂”, *Phys. Rev. B* 80(3), 035202 (2009). <http://dx.doi.org/10.1103/PhysRevB.80.035202>
- [39] J. M. D. Coey, A. P. Douvalis, C. B. Fitzgerald and M. Venkatesan, “Ferromagnetism in Fe-doped SnO₂ thin films”, *Appl. Phys. Lett.* 84(8), 1332-1334 (2004). <http://dx.doi.org/10.1063/1.1650041>
- [40] F. Esch, S. Fabris, L. Zhou, T. Montini, C. Africh, P. Fornasiero, G. Comelli and R. Rosei, “Electron localization determines defect formation on ceria substrates”, *Science*, 309(5735), 752-755 (2005). <http://dx.doi.org/10.1126/science.1111568>

- [41] M. Radovic, Z. Dohcevic-Mitrovic, N. Paunovic, M. Scepanovic, B. Matovic and Z. V. Popovic, "Hydrothermal synthesis of CeO₂ and Ce_{0.9}Fe_{0.1}O₂ nanocrystals", *Acta Phys. Pol. A* 116(4), 614-617 (2009).
- [42] V. Fernandes, P. Schio, A. J. A. de. Oliveira, W. H. Schreiner, and J. Varalda and D. H. Mosca, "Loss of magnetization induced by doping in CeO₂ films", *J. Appl. Phys.* 110(11), 113902 (2011). <http://dx.doi.org/10.1063/1.3664764>
- [43] S. Colis, A. Bouaine, G. Schmerber, C. Ulhaq-Bouillet, A. Dinia, S. Choua and P. Turek, "High-temperature ferromagnetism in Co-doped CeO₂ synthesized by the coprecipitation technique", *Phys. Chem. Chem. Phys.* 14(20), 7256-7263 (2012). <http://dx.doi.org/10.1039/c2cp23973f>